Pulse-width-dependent subluminal and superluminal propagation in highly doped erbium fibers

Francisco Arrieta-Yáñez,* Eduardo Cabrera-Granado, José M. Ezquerro, Oscar G. Calderón, and Sonia Melle

Departamento de Óptica, Escuela Universitaria de Óptica, Universidad Complutense de Madrid, C/Arcos de Jalón 118, 28037 Madrid, Spain
**Corresponding author: franarrieta@fis.ucm.es*

Received November 15, 2010; revised March 9, 2011; accepted March 13, 2011; posted March 22, 2011 (Doc. ID 138234); published April 19, 2011

We experimentally and theoretically study the propagation of a 1536 nm light pulse superposed on a continuous wave background in a highly doped erbium fiber pumped at 977 nm. We observe a transition from subluminal to superluminal propagation with the pulse bandwidth. Furthermore, an improvement of the pulse delay and pulse distortion when increasing the pulse peak and keeping constant the background power is reported. These results are due to the relation between the pump-broadened transparency hole (induced by the coherent population oscillations) and the competition between gain and absorption along the fiber.

OCIS codes: 060.2330, 060.2410, 190.4370.

1. INTRODUCTION

Slow and fast light propagation phenomena, that involve group velocities much lower or much faster than c, have become very important in the last years in the fields of quantum optics and nonlinear optics. Potential applications include all-optical communication networks [1], and optical sensing [2,3]. From the wide spectra of slow/fast light techniques, the so-called coherent population oscillations (CPOs) present the advantage of room-temperature realization. CPOs occur when a medium is illuminated by a strong ("control") beam and a weak ("probe") beam, slightly detuned with the control beam. Their frequencies must lie within an absorption band of the medium. This causes an oscillation of the population at the beat frequency, which induces a reduction of the absorption that the probe beam experiences. This can be seen as a spectral hole in the absorption spectrum of the probe field. The width of this hole is in the order of the inverse of the excited level lifetime. According to the Kramers–Kronig relations, the refractive index varies rapidly in the frequency range of the spectral hole, presenting a high-dispersion spectral zone and leading to slow light for the probe beam. The experimental realization is usually performed with amplitude-modulated optical beams and Gaussian-shaped light pulses superimposed on a continuous background, with a modulation frequency or pulse bandwidth in the range of the inverse of the excited level lifetime. By means of an additional pump to a higher energy level, the same phenomenon induces a hole in the gain spectrum, leading to anomalous dispersion and fast light for the probe beam.

The first experimental realization of slow light by means of this technique was performed by Bigelow *et al.* [4] in a ruby crystal rod. CPO-based slow and fast light has been observed in a variety of materials such as alexandrite [5], erbium-doped fibers (EDFs) [6,7], biological thin films [8], and semiconductor waveguides (electroabsorbers [9] and semiconductor optical amplifiers [10]). Slow and fast light experiments in optical fibers are especially interesting for their integration in communication networks. Fibers also allow propagation of light through the slow light medium in longer distances, which helps to produce greater delays. Optical fibers doped with Er^{3+} ions (EDFs) are widely used in telecommunications as amplifiers of 1550 nm signals by means of optical pumping. In the past several years, several works have studied the sub- and superluminal propagation of signals around this wavelength through EDFs [11–13]. In particular, Melle *et al.* observed a transition from subluminal to superluminal propagation in amplitude-modulated signals propagated through highly doped erbium fibers (HEDFs) solely upon an increase in the modulation frequency [12]. Other works have investigated the control of the distortion of superluminal light pulses caused by the interplay between pulse broadening and compression [14,15].

Following these works, here we study the propagation of light pulses superposed on a continuous wave (cw) background in HEDFs, where a strong gain and absorption take place along the fiber. We show that, for certain conditions, a variation of the propagation regime (from subluminal to superluminal) takes place when varying the pulse bandwidth. We examine the distortion of the pulses during this transition. To simulate the results, we have used a rate equation analysis. We investigate also the possibility of improving the delay and the available bandwidth by controlling the pulse-peak-to-background power ratio. The variation of the propagation regime with the pulse bandwidth has also been obtained using a cascade system formed by an amplifier and an absorber, both short enough to work in the undepleted propagation regime, i.e., to neglect gain and absorption of the beams in both fibers.

2. THEORETICAL MODEL

To simulate the propagation of a signal beam (1536 nm) and a copropagating pump beam (977 nm) along the EDF, we have followed a rate equation analysis [6,16]. Erbium ions can be modeled as a three-level system, consisting of a ground level ($^4I_{15/2}$), a metastable level ($^4I_{13/2}$) with a lifetime of $\tau \sim 10.5$ ms

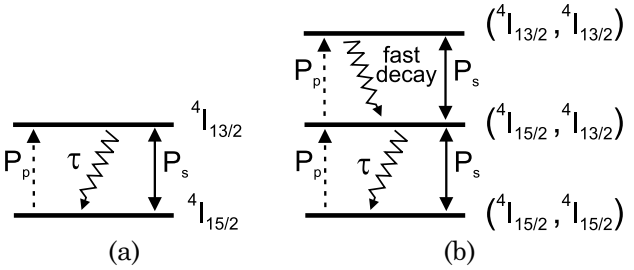

Fig. 1. Energy levels for (a) isolated Er ions and (b) paired ions.

and a transition wavelength with a ground level of 1536 nm, and a third level $^4I_{11/2}$ (transition wavelength of 977 nm) used to pump the system. Assuming a fast decay of the pump level, we can describe the ions as a two-level system [see Fig. 1(a)], being the population densities of the ground level and the metastable level n_1 and n_2, respectively (normalized to the total density ρ).

Pair quenching effects (inhomogeneous upconversion) are the main cause of gain degradation in HEDFs [17]. Because of nonuniform erbium ions distribution, energy transfer can occur between two adjacent excited paired ions. Following the model developed by Li *et al.* [18], and later used by Calderón *et al.* [19] to study the effect of ion pairs on slow and fast light, we divide the erbium ions into two groups, isolated ions and paired ions (with a fraction of ion pairs in the total ion concentration given by κ). Ion pairs can be described as a three level system [see Fig. 1(b)]: ground level ($^4I_{15/2}$, $^4I_{15/2}$), intermediate level ($^4I_{15/2}$, $^4I_{13/2}$) and upper level ($^4I_{13/2}$, $^4I_{13/2}$), with population densities n_{11}, n_{12} and n_{22}, respectively (all of them normalized to ρ). As decay from the upper level to the intermediate level is very fast compared with τ, we can consider only the ground and intermediate levels ($n_{11}+n_{12}\simeq\kappa$) [19]. The rate equations for n_1 and n_{11} are

$$\frac{\partial n_1}{\partial t}=\frac{(1-2\kappa)-n_1}{\tau}+\frac{1}{\tau}\frac{P_s}{2}(1-2\kappa-2n_1)-\frac{P_p n_1}{\tau}, \quad (1)$$

$$\frac{\partial n_{11}}{\partial t}=\frac{\kappa-n_{11}}{\tau}+\frac{1}{\tau}\frac{P_s}{2}(\kappa-2n_{11})-\frac{P_p n_{11}}{\tau}, \quad (2)$$

where P_s and P_p are the 1536 nm signal power and the 977 nm pump power, respectively, normalized to their respective saturation powers P_s^{sat} and P_p^{sat}. The propagation equations of the signal and pump powers along the fiber can be described with the following equations that take into account the inhomogeneous upconversion effects:

$$\frac{\partial P_s}{\partial z}+\frac{n_{gs}}{c}\frac{\partial P_s}{\partial t}=\alpha_s[1-2\kappa-2n_1-n_{11}]P_s, \quad (3)$$

$$\frac{\partial P_p}{\partial z}+\frac{n_{gp}}{c}\frac{\partial P_p}{\partial t}=-\alpha_p[n_1+\kappa]P_p. \quad (4)$$

Here α_s and α_p are the absorption coefficients for the signal and pump beams, and n_{gs} and n_{gp} are the group indices of the signal and pump in the fiber glass, respectively. The signal power envelope at the beginning of the fiber ($z=0$) is a Gaussian pulse superposed on a cw background, $P_s^{\mathrm{in}}(t)=P_{bg}+P_m(t)=P_{bg}+P_{\mathrm{peak}}\exp[-(t/T_0)^2]$, with a FWHM given by $\tau_{\mathrm{in}}=2T_0(\log 2)^{1/2}$. Following the work by Wen and Chi [20], we spectrally analyzed the problem by decomposing the pulse power envelope in its modulation frequency components: $P_s(t)=P_{bg}+P_m(t)=P_{bg}+\int\tilde{P}_m(\Omega)\exp(-i\Omega t)\mathrm{d}\Omega$, where $\tilde{P}_m(\Omega)$ is the amplitude of each power modulation term. Assuming that the modulation in the signal power will induce a modulation in the ground level population along the fiber, we can write the ground level populations as

$$n_1(t)=n_{1bg}+n_{1m}(t)=n_{1bg}+\int\tilde{n}_{1m}(\Omega)e^{-i\Omega t}\mathrm{d}\Omega, \quad (5)$$

$$n_{11}(t)=n_{11bg}+n_{11m}(t)=n_{11bg}+\int\tilde{n}_{11m}(\Omega)e^{-i\Omega t}\mathrm{d}\Omega, \quad (6)$$

where $\tilde{n}_{1m}(\Omega)$ and $\tilde{n}_{11m}(\Omega)$ are the amplitudes of the population oscillations of each spectral component. Here, we consider that $P_m\ll P_{bg}$, and hence, the modulation terms can be treated as perturbations. This is the most common situation in CPO-based slow light [4,6]. Furthermore, pump power temporal variation will be induced by the population oscillations. This phenomenon, which is called temporal pump depletion (TPD), produces higher absorption of the pump beam [20]. We have checked that our experimental results are reasonably well explained without including in our model the TPD effect.

From Eqs. (5) and (6), and the rate Eqs. (1) and (2), we obtain the stationary population and the population oscillations amplitudes equating the terms of the same order:

$$n_{1bg}=\frac{(1-2\kappa)(1+P_{bg}/2)}{\omega_c}, \quad (7)$$

$$n_{11bg}=\frac{1+P_{bg}/2}{\omega_c}\kappa, \quad (8)$$

$$\tilde{n}_{1m}(\Omega)=\frac{(1-2\kappa)\tilde{P}_m(\Omega)/2-n_{1bg}\tilde{P}_m(\Omega)}{\omega_c-i\Omega\tau}, \quad (9)$$

$$\tilde{n}_{11m}(\Omega)=\frac{(\tilde{P}_m(\Omega)/2)\kappa-n_{11bg}\tilde{P}_m(\Omega)}{\omega_c-i\Omega\tau}, \quad (10)$$

where $\omega_c\equiv 1+P_{bg}+P_p$ is the so-called "CPO central frequency," a dimensionless frequency that roughly gives the available bandwidth to obtain signal delay or advancement. From these results and the power propagation [Eqs. (3) and (4)], it is straightforward to obtain the propagation equations for the signal background and pump powers. The terms with n_{gs} and n_{gp} in Eqs. (3) and (4) are negligible, because the delay from these contributions is much smaller than the delay caused by CPO. Therefore, these equations read

$$\frac{\partial P_{bg}}{\partial z}=\alpha_s[1-2\kappa-2n_{1bg}-n_{11bg}]P_{bg}, \quad (11)$$

$$\frac{\partial P_p}{\partial z}=-\alpha_p(n_{1bg}+\kappa)P_p, \quad (12)$$

and for each modulation frequency term of the signal power envelope:

$$\frac{\partial \tilde{P}_m(\Omega)}{\partial z} = C_s \tilde{P}_m(\Omega), \tag{13}$$

where the coefficient C_s is given by

$$C_s = \frac{\alpha_s}{\omega_c}\left[(P_p - 1) + \kappa\left(1 - \frac{P_{bg}}{2} - 2P_p\right) - \frac{\left[(P_p - 1) + \frac{3\kappa}{2}(1 - P_p)\right]P_{bg}}{\omega_c - i\Omega\tau}\right]. \tag{14}$$

The pulse at the end of the fiber, $P_m(t, z = L)$ is obtained from the inverse Fourier transform of the output power envelope of the modulation frequency components $\tilde{P}_m(\Omega, z = L)$: $P_m^{\text{out}} = \int \tilde{P}_m^{\text{out}} \exp(-i\Omega t)\mathrm{d}\Omega$. The time delay is calculated as the time difference between the maximum of the delayed pulse and the maximum of the reference pulse. Because $C_s(\Omega)$ is complex, the imaginary (real) part stands for a phase delay (absorption) of each modulation frequency component of the signal power envelope. By neglecting the variation of the signal and pump along the fiber, i.e., the undepleted approximation, the delay is given by $t_d \approx \mathrm{Im}(C_s(\Omega))z/\Omega$. Note that the achieved delay increases with fiber length.

3. RESULTS AND DISCUSSION

The experimental setup consists basically of an EDF in the forward-pumped configuration. Details have been described in [13], Fig. 2. It allows us to control the initial pulse width (τ_{in}), which is given as the FWHM, and the pulse-peak-to-background power ratio. Pulses are propagated through an Al_2SiO_5-glass-based EDF with ion density of $\rho = 8.7 \times 10^{25}\,\text{m}^{-3}$ and 1 m long. Delay/advancement is measured as the time difference between the peaks of a reference pulse (which travels through nondoped fibers) and the pulse propagated through the EDF. Delay/advancement time is normalized to the reference pulse width (FWHM), giving the so-called fractional delay F, defined as $F < 0$ for delay and $F > 0$ for advancement.

A. Subluminal to Superluminal Transition with Pulse Width

We have measured the pulse delay varying τ_{in} from 0.33 to 100 ms. This range covers the width of the CPO hole. In the following, we use a small amplitude pulse compared to the background. In particular, we use a pulse-peak-to-background power ratio of $P_{\text{peak}}/P_{bg} = 0.2$. When the pump is not present, all pulses propagate at subluminal velocities (not shown), as has been previously reported [6,11]. Furthermore, pulses with a few milliseconds of width show the largest slow light effect. By pumping the fiber, as we are using fibers with a high ion concentration, strong absorption of the pump occurs so that gain will be only achieved in the front part of the fiber. Moreover, the CPO hole will broaden with pump power. Therefore, in this first region, pulse advancement will take place, being greater for shorter temporal pulses. In Fig. 2(a), we plot the fractional delay versus the inverse of τ_{in} for different pump powers and for a signal background power of 3.5 mW. A transition from subluminal to superluminal propagation with the pulse width takes place. That is, pulses longer than 1.5 ms propagate subluminally, while shorter pulses propagate at superluminal velocities. A high pump power value is needed to achieve a strong enough gain in the front part of the fiber to be comparable to the absorption that appears along the rest of the fiber, allowing a transition from subluminal to superluminal propagation. In this particular case, a pump power of 96 mW is needed to observe this transition. In Fig. 2(b), we plot the fractional delay versus the inverse of τ_{in} for different signal background powers and for a pump power of 107 mW. For small signal background powers, we observe such a transition from subluminal to superluminal velocities [see circles in Fig. 2(a), corresponding to a signal background power of 1.8 mW]. However, for high signal background powers [see triangles in Fig. 2(a), which correspond to a signal background power of 6.8 mW], we see only subluminal propagation. For this high signal power, saturation gain occurs so that signal background suffers small amplification. Thus, the small advancement achieved in the front part of the fiber will be canceled out by the delay achieved in the rest of the fiber so that all pulses will show a net delay.

We have simulated these results with the previous perturbative model [Eqs. (11)–(13)]. We have used the measured powers as initial values, keeping insertion losses as fitting parameters. We obtained 10% and 80% losses for the signal and the pump, respectively. The saturation powers for the signal and pump beams are $P_s^{\text{sat}} \simeq 0.36\,\text{mW}$ and $P_p^{\text{sat}} \simeq 1.3\,\text{mW}$, respectively. The unsaturated absorption coefficients for the same beams are $\alpha_s \simeq 0.21\,\text{cm}^{-1}$ and $\alpha_p \simeq 0.18\,\text{cm}^{-1}$. These values are consistent with the ones used in previous works [6,11]. The fraction of ion pairs in the total ion concentration is set to $\kappa = 0.2$ (a similar value to the one used in previous works for HEDFs [19]). The simulation results, depicted in Fig. 2 (solid

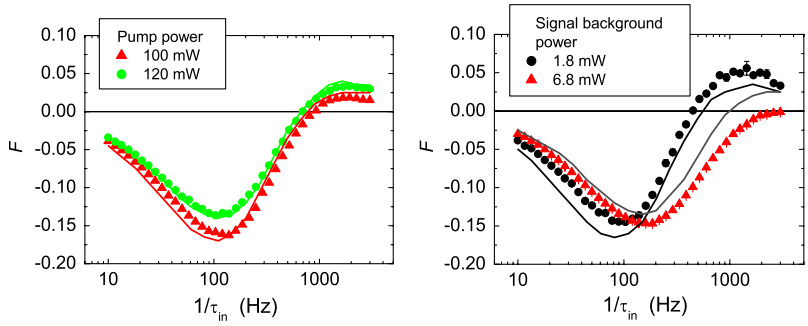

Fig. 2. (Color online) Experimental (symbols) and simulated (curves) fractional delay as a function of inverse of the pulse width (FWHM). (a) Different pump powers and a fixed signal background power (3.5 mW). (b) Different signal background powers and a fixed pump power (107 mW).

curves), reproduce well the change from subluminal to superluminal propagation with the pulse width.

The peculiar phenomena described above can be explained as a combined effect of the spectral hole broadening with pump power and the change from gain to absorption of the signal along the fiber. The background signal power and the pump power distribution along the fiber determine the delay of the pulses in different sections of the fiber. The final result is a modified gain profile. The shape of the gain curve will be further investigated in Subsection 3.A.1. The effects of the modified gain profiles on light propagation have been previously analyzed in other techniques such as stimulated Brillouin scattering [21]. In the initial part of the fiber, pulses are advanced since gain is dominant because a strong pump is present. In particular, broad-spectrum pulses ($1/\tau_{\text{in}} \simeq$ 1000 Hz) suffer the largest fractional advancement due to the pump-broadened spectral hole. In the final part of the fiber, the pump is almost completely absorbed due to the high ion concentration. Thus, pulse delay occurs in this part of the fiber. In particular, narrow-spectrum pulses ($1/\tau_{\text{in}} \simeq 100$ Hz) suffer the largest fractional delay. For the case depicted in Fig. 2(a) (triangles), absorption is dominant in the whole length of the fiber, causing great delays for all bandwidths. For the rest of the curves shown in Figs. 2(a) and 2(b), where a transition of the propagation regime takes place, the initial power values are such that the gain region in the initial part of the fiber and the absorptive region in the final part of the fiber are equally significant. This leads to a net advancement for short pulses, while long pulses will present a net delay at the output of the fiber.

1. Cascade System

In order to explain more clearly the change in the propagation regime from subluminal to superluminal with the pulse width and find possible implementations of slow light devices based on this effect, we have reproduced this behavior with an undepleted equivalent system, which makes use of short fibers where attenuation and amplification of the signal background and pump powers can be neglected (undepleted approximation). This allows us to explain the results with an analytical model and gives us a better understanding of the phenomenon.

As we said before, the phenomenon observed in Fig. 2 is due to the competition between gain and absorption along the fiber. In Fig. 3(a) we have plotted the powers profiles (normalized with their saturation powers) along 1 m long fiber, for the particular values corresponding to those in Fig. 2(b) (circles), where a change from subluminal to superluminal propagation was observed. Note that the pump is almost totally absorbed in the first half of the fiber. This strong absorption is due to the high Er^{3+} concentration and the inhomogeneous upconversion processes caused by the presence of ion pairs (PIQ). Let us imagine a simple and equivalent configuration that consists of two short fibers, one pumped (amplification stage, EDFA), and the other one without the pump (absorbing stage, EDF), as depicted in Fig. 3(b). The device was experimentally implemented with two EDFs of length $L = 10$ cm. In the first stage, the 1536 nm pulse superposed on the signal background and the 980 nm pump were copropagated. We measured the pulse delay at the output of this fiber. Then we used wavelength division multiplexing to extract the pump beam at the output of this first stage, and we introduced the 1536 nm signal into the second EDF. We again measured the pulse delay at the output of the device. In Fig. 4, the fractional delay is plotted against the spectral width of the initial pulses for a pump power of 39 mW and a signal background power of 2 mW (triangles). The same measurement without the second stage is also plotted in the same figure (circles). We observe that only superluminal propagation takes place at the output of the first stage. However, at the output of the second fiber, a change of the propagation regime with the pulse width is observed, as occurs in the experiments shown before, where we used one long fiber. This simple experiment allows us to confirm that the main reason for the change in the propagation regime with the pulse spectral width is the competition between gain and absorption occurring along the system. This "cascade" configuration makes possible the control of the delay in CPO delay lines, and it has been previously used in semiconductor-based CPOs [22,23].

From Eq. (13), the derivation of the results is straightforward. Assuming the undepleted approximation and neglecting pair-quenching effects, the pulse spectrum at the output of the device will be given by $\tilde{P}_m^{\text{out}} \simeq \tilde{P}_m^{\text{in}} e^{\alpha L} e^{-i\varphi}$, where α is the total absorption/gain coefficient and φ is the total phase delay accumulated along the two stages:

$$\varphi = L\alpha_s P_{bg}\Omega\tau\left[\frac{P_p - 1}{\omega_{c_1}(\omega_{c_1}^2 + (\Omega\tau)^2)} - \frac{1}{\omega_{c_2}(\omega_{c_2}^2 + (\Omega\tau)^2)}\right]. \quad (15)$$

Here $\omega_{c_1} \equiv 1 + P_{bg} + P_p$ and $\omega_{c_2} \equiv 1 + P_{bg}$ are the CPO central frequencies in the first and second stages, respectively, and

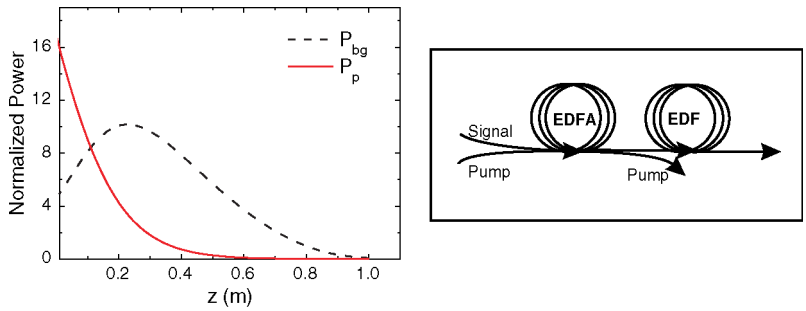

(a) (b)

Fig. 3. (Color online) (a) Simulated signal background (dashed curve) and pump (solid curve) power profiles along 1 m long fiber, normalized to their respective saturation powers. Initial values are 1.8 (signal background power) and 107 mW (pump power). (b) Schematic diagram of the cascade system.

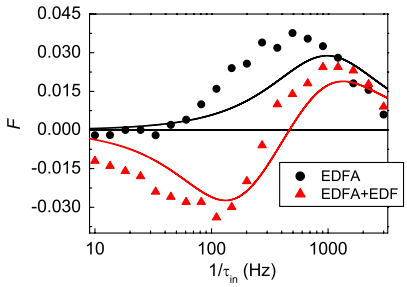

Fig. 4. (Color online) Fractional delay versus the inverse of the pulse width in one amplification stage (circles) and in two stages, amplification and absorbtion (triangles). The signal background power was set to 2 mW for both measurements, and the pump power was set to 39 mW in the amplification stage. The theoretical result given by Eq. (17) is also plotted (solid curves).

L is the fiber length of each stage. Furthermore, the total absorption/gain coefficient α is given by

$$\alpha = \alpha_s \left[\frac{P_p - 1}{\omega_{c_1}} - \frac{P_{bg}(P_p - 1)}{\omega_{c_1}^2 + (\Omega\tau)^2} - \frac{1}{\omega_{c_2}^2} + \frac{P_{bg}}{\omega_{c_2}^2 + (\Omega\tau)^2} \right]. \tag{16}$$

In order to compare the results of our model with the experimental results, we calculate the inverse Fourier transform of the pulse power spectrum and we estimate the delay as the difference between the maximum of the delayed pulse and the reference pulse. The simulations reproduce the change in the propagation regime (not shown). Furthermore, we have checked that in order to reproduce the experimental results, distortion caused by absorption or gain ($e^{\alpha L}$) can be neglected. Following this approximation, we have analytically solved the inverse Fourier transform to obtain the pulse time delay:

$$t_d = \frac{\alpha_s(P_p - 1)P_{bg}}{\omega_{c_1}} \frac{1}{\omega_{c1}^2 + \frac{24\ln 2}{\tau_{\text{in}}^2}} - \frac{\alpha_s P_{bg}}{\omega_{c_2}} \frac{1}{\omega_{c_2}^2 + \frac{24\ln 2}{\tau_{\text{in}}^2}}. \tag{17}$$

In Fig. 4 we have plotted the analytical F (solid curves) showing good agreement with the experimental results. The analytical curve for the EDFA stage shows a small shift in the pulse width where the maximum advancement is obtained as well as a slight increase in the amount of advancement achieved. These small discrepancies are due to the depletion of the pump beam that occurs in highly doped fibers, even for this small length, that is obviated in the undepleted approximation.

Let us analyze in more detail the spectral response of each stage. In Fig. 5 we plot the absorption/gain coefficient α (a) and the phase delay φ (b) as a function of $\Omega\tau$ for the EDFA stage (dashed curve), EDF stage (dotted curve), and cascade system (solid curve) using the same power values as in Fig. 4. Thus, each frequency component of the pulse propagating through the fiber will experience the absorption shown in Fig. 5(a) and will propagate with a refractive index that is proportional (with a negative sign) to the phase delay shown in Fig. 5(b). The total absorption is the contribution of the absorption generated in each stage of the system. In the EDFA stage, a broad hole in the gain spectrum is obtained, while in the EDF stage a narrow hole in the absorption spectrum occurs. As a result, the total gain spectrum shows a broad hole and a narrow antihole.

In Fig. 6 we have plotted the total index (with arbitrary dimensions) (solid curves) together with two pulses with different spectral widths (dashed curves). A spectrally narrow pulse will be inside the normal dispersion region so that every frequency will be delayed. When the pulse gets spectrally wider, it exceeds the normal dispersion region. Most of the spectral components will observe the broad hole in the gain spectrum propagating in a superluminal regime. Note that a wide spectral pulse will suffer distortion, because the central frequencies will be inside the normal dispersion regime, while the lateral frequencies will propagate at superluminal velocities. Therefore, a description of its propagation based only in the delay between the pulse peaks is incomplete. In the next section we study pulse broadening and distortion for a case where a change in the propagation regime is observed.

2. Pulse Distortion

Practical applications of slow and fast light must take into account pulse broadening and pulse narrowing due to the propagation in the slow/fast light system. The gain spectrum of EDFAs shows a CPO hole with a characteristic width of 100 Hz. Thus, the high-frequency components of the pulse would be amplified, causing a narrowing of the pulse in time domain. On the other hand, pulse broadening would occur due to the saturation of the amplifier gain. These competing mechanisms result in the distortion of the pulse. In this section we study the behavior of the pulse width, and the distortion of the delayed/advanced pulses as the input pulse spectrum gets broader. We used a pump of 107 mW and a signal background of 1.8 mW. This case corresponds to the one

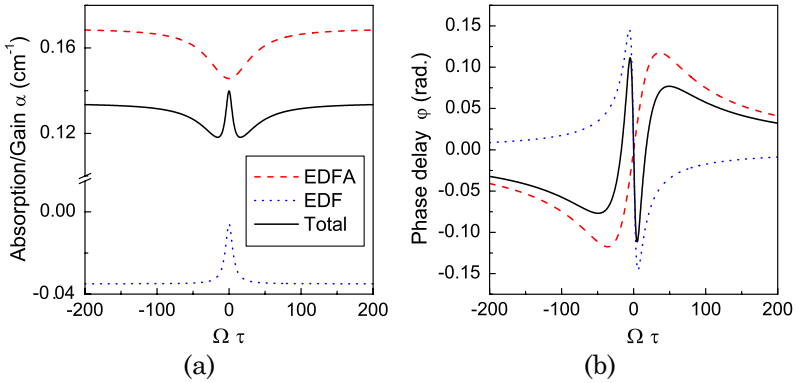

Fig. 5. (Color online) (a) Absorption and (b) phase delay for a pumped EDF (dashed curve), a nonpumped EDF (dotted curve) and for the whole system EDFA + EDF (solid curve) as a function of $\Omega\tau$.

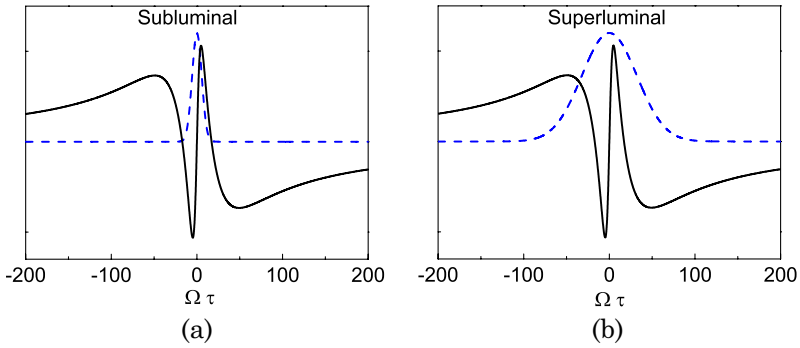

Fig. 6. (Color online) Spectrum of two pulses (dashed curves) superposed to the refractive index of the system (solid curves). (a) Spectrally narrow pulse (subluminal). (b) Spectrally broad pulse (superluminal).

shown in Fig. 2(b) (circles), where a transition from subluminal to superluminal propagation with the pulse width was observed. We show in Fig. 7 three representative pulses where we can observe the different propagation regimes and the distortion appearing in each case. The narrow-spectrum pulses, which are delayed, suffer broadening [see Figs. 7(a) and 7(b)]. The broad-spectrum pulses, which are advanced, suffer compression [see Figs. 7(c) and 7(d)]. Broadening and compression are computed by means of the pulse FWHM ratio, which accounts for the distortion of the remaining Gaussian part of the pulse. In Fig. 8(a) we have plotted the ratio between the delayed and the reference pulse widths (FWHM), as a function of $1/\tau_{\text{in}}$. We observe how pulse broadening occurs mainly for subluminal propagated pulses. For short pulses (less than 2.2 ms, with superluminal propagation) we have narrowing. This is explained in the frequency domain, because the pulse spectral width exceeds the CPO hole in the gain profile. Thus, the wings of the pulse are amplified, and the pulse spectrum gets broadened. Amplification of the wings induces a "tail" after the pulse [see Figs. 7(c) and 7(d)] that distorts the pulse.

To account for this distortion, we use the metric proposed by Bigelow *et al.* in [24] as the deviation the pulse has at the end of the system compared to its initial shape:

$$D = \left(\frac{\int_{-\infty}^{+\infty} ||P_{\text{out}}(t+t_d)|^2 - |P_{\text{in}}(t)|^2|\mathrm{d}t}{\int_{-\infty}^{+\infty} |P_{\text{out}}(t+t_d)|^2\mathrm{d}t}\right)^{1/2} - \left(\frac{\int_{-\infty}^{+\infty} ||P_{\text{in}}(t+\delta t)|^2 - |P_{\text{in}}(t)|^2|\mathrm{d}t}{\int_{-\infty}^{+\infty} |P_{\text{out}}(t+\delta t)|^2\mathrm{d}t}\right)^{1/2}, \tag{18}$$

where P_{in} and P_{out} are the normalized pulse envelopes at the beginning and at the end of the fiber, respectively; t_d is the delay time; and δt is the temporal resolution of the experimental data. In Fig. 8(b) we have plotted the measured and simulated distortion for the case depicted in Fig. 2(b) (circles). It is noticeable that its greater value occurs for the most advanced pulse. Pulse distortion increases as the input pulse is shorter, that is, when it exceeds the dip in the gain profile.

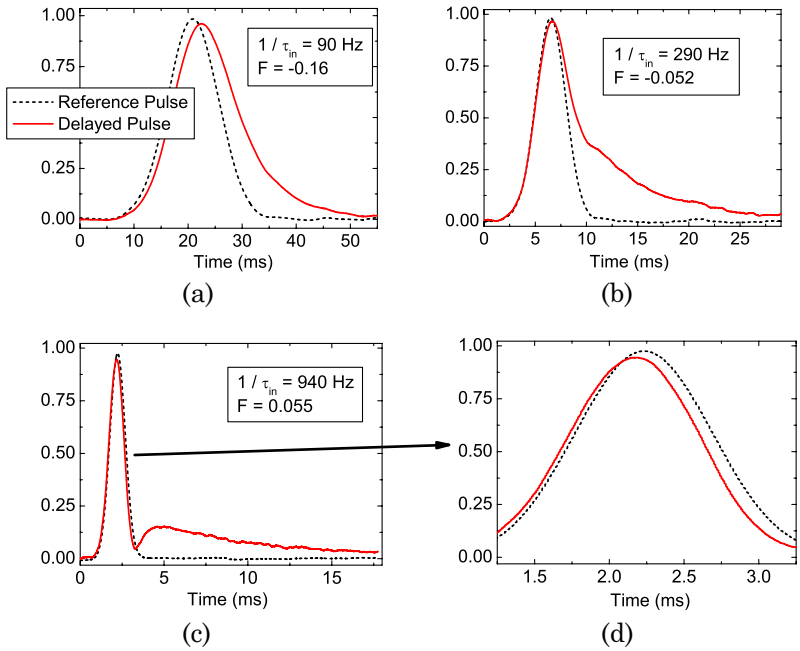

Fig. 7. (Color online) Representative delayed and advanced normalized pulses (solid curve) with their respective reference pulses (dashed curve), for a signal background power of 1.8 mW and a pump power of 107 mW: (a) $1/\tau_{\text{in}} = 90$ Hz, (b) $1/\tau_{\text{in}} = 290$ Hz, (c) $1/\tau_{\text{in}} = 940$ Hz, and (d) magnification of the Gaussian part of the pulse of (c).

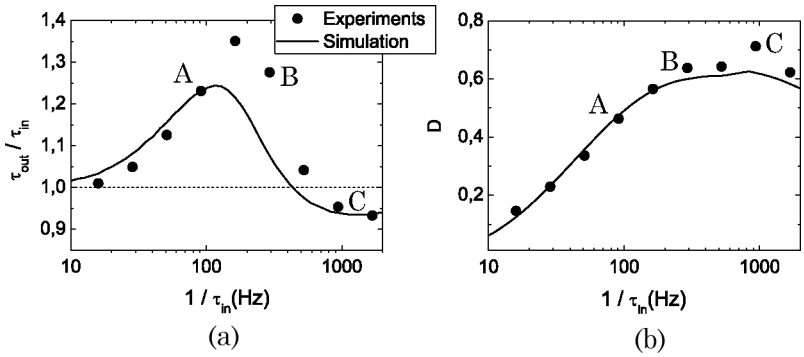

Fig. 8. Measured (dots) and simulated (line) (a) pulse width ratio and (b) distortion versus the inverse of the input pulse width. Both figures correspond to initial powers of 1.8 (background signal) and 107 mW (pump). Pulses (a), (b), and (c) from Fig. 7 correspond to points A, B, and C in this figure.

B. Influence of Pulse Height

High pulse-peak powers compared with the signal background power have not been considered in most previous CPO works [6]. However, recent studies [11,25] have obtained interesting results in subluminal and superluminal pulse propagation when the pulse-peak power is arbitrarily high. In this situation, pulse interaction with the medium is fully nonlinear and it is not only seen as a probe. Macke *et al.* [25] showed theoretically, using a saturable absorption approach, that larger pulse-peak powers provided larger fractional delays. Moreover, recent studies [11,14] demonstrate that pulse distortion can be reduced by modifying the pulse-peak-to-background power ratio. Specifically, in [14], Shin *et al.* measured the deformation of advanced pulses for different values of the background power P_{bg}, while keeping constant the pulse-peak power P_{peak} to 55 μW. They concluded that the pulse-peak-to-background power ratio can be used as a free parameter to minimize pulse distortion. They found that fractional advancement was independent of the pulse-peak-to-background power ratio, for values of P_{peak}/P_{bg} above 0.4.

In this section we study the influence of pulse-peak-to-background power ratio on the delay. Here in this work, and in contrast to the above-mentioned studies [11,14], we keep constant the background power (to a value greater than the saturation power of the EDFA) and vary the pulse-peak power. In particular, the pulse-peak-to-background power ratio varies from 0.2 to 25. This allows us to look beyond the approximation that considers the pulse as a probe. We have found that the propagation of pulses with a peak power larger than the background power leads to greater fractional delays/advancements and increases the available bandwidth as the pulse-peak power increases.

We carried out a series of experiments where we measured F, varying the pulse width from 0.33 to 100 ms, for different values of P_{peak}/P_{bg}, from 0.2 to 25. We kept a constant background power of 0.9 mW and varied the pulse-peak power. The pump power is set to 140 mW. For these values of pump and background powers, and for small values of the pulse-peak-to-background power ratio, narrow-spectrum pulses ($1/\tau_{\text{in}} \simeq 100$ Hz) suffer delay, and broad-spectrum pulses ($1/\tau_{in} \simeq 1000$ Hz) suffer advancement, as shown in Subsection 3.A. We focus our attention on the range of pulse widths where subluminal propagation occurs. In Fig. 9(a) we have plotted the maximum fractional delay we have obtained varying pulse width (FWHM) for each value of the pulse-peak-to-background power ratio. The pulse width (FWHM) where the maximum fractional delay occurs (called optimum pulse width) is also plotted against the pulse-peak-to-background power ratio [see Fig. 9(b)]. In order to properly reproduce these experimental results, integration of the complete model shown in Eqs. (1) and (2) without further approximations has been carried out. The curves in Fig. 9 show a good agreement with the experimental data (symbols). We observe that with a pulse-peak-to-background power ratio of 25, we can obtain fractional delays two times larger than the one obtained with a power ratio of 0.2 (from $F = -0.084$ to $F = -0.174$). The available bandwidth also increases with the pulse-peak-to-background power ratio. There is a difference of 1 order of magnitude in the spectral width of the pulse that suffers the maximum fractional delay for the values of P_{peak}/P_{bg}

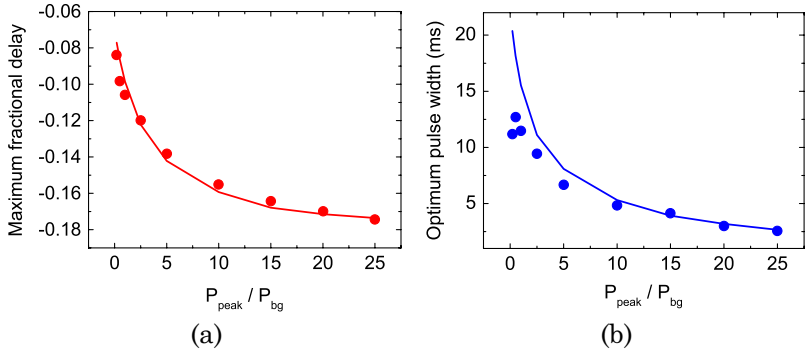

Fig. 9. (Color online) (a) Experimental (symbols) and simulated (curve) maximum fractional delay versus P_{peak}/P_{bg}. (b) Experimental (symbols) and simulated (curve) optimum pulse width, i.e., the pulse width where the maximum fractional delay is achieved versus P_{peak}/P_{bg}.

measured (from $1/\tau_{\text{in}} = 90\,\text{Hz}$ for a power ratio of 0.2 to $1/\tau_{\text{in}} = 390\,\text{Hz}$ for a power ratio of 25). This is expected, as the pulse-peak power is involved along with the background power in the broadening of the CPO hole. The fractional delay increase can be explained by a higher saturation of the absorption by the leading edge of the pulse. By integration of the complete model, we found that a saturation of the increase of the fractional delay with the pulse-peak-to-background power ratio occurs for $P_{\text{peak}}/P_{bg} > 40$.

4. CONCLUSIONS

Pulse propagation in EDFAs has been experimentally investigated. Pulses of different widths have been propagated through a very highly doped erbium fiber. A transition in the propagation regime (from subluminal to superluminal) with the pulse width is reported. This is explained by the abrupt change in the signal and pump power profiles along the fiber, caused by the high absorption. We have simulated these results with a rate equation model. We reproduce the same behavior with a more comprehensive experimental setup, consisting in two stages, one pumped fiber followed by another one without the pump. This simple model allows us to calculate the analytical delay of both steps. Finally, we found an improvement of the pulse delay and the available bandwidth when increasing the pulse-peak power while keeping constant the background power. This is explained by the contribution of the pulse to the nonlinear saturation of the absorption.

ACKNOWLEDGMENTS

This work has been supported by the Ministerio de Educación y Ciencia (FIS2007-65382) and the Banco Santander–Central Hispano/Universidad Complutense de Madrid (GR58/08: 910133-1030). F. Arrieta-Yáñez appreciates the financial support from the Consejería de Educación de la Comunidad de Madrid and the European Social Fund. We would like to thank professors M. A. Antón and F. Carreño for fruitful discussions and scientific support.

REFERENCES

1. R. W. Boyd, D. J. Gauthier, and A. L. Gaeta, "Applications of slow light in telecommunications," Opt. Photon. News **17**, 18–23 (2006).
2. C. Peng, Z. Li, and A. Xu, "Rotation sensing based on a slow-light resonating structure with high group dispersion," Appl. Opt. **46**, 4125–4131 (2007).
3. Z. Shi, R. W. Boyd, D. J. Gauthier, and C. C. Dudley, "Enhancing the spectral sensitivity of interferometers using slow-light media," Opt. Lett. **32**, 915–917 (2007).
4. M. S. Bigelow, N. N. Lepeshkin, and R. W. Boyd, "Observation of ultraslow light propagation in a ruby crystal at room temperature," Phys. Rev. Lett. **90**, 113903 (2003).
5. M. S. Bigelow, N. N. Lepeshkin, and R. W. Boyd, "Superluminal and slow light propagation in a room-temperature solid," Science **301**, 200–202 (2003).
6. A. Schweinsberg, N. N. Lepeshkin, M. S. Bigelow, R. W. Boyd, and S. Jarabo, "Observation of superluminal and slow light propagation in erbium-doped optical fiber," Europhys. Lett. **73**, 218–224 (2006).
7. G. M. Gehring, A. Schweinsberg, C. Barsi, N. Kostinski, and R. W. Boyd, "Observation of backward pulse propagation through a medium with a negative group velocity," Science **312**, 895–897 (2006).
8. P. Wu and D. V. G. L. N. Rao, "Controllable snail-paced light in biological bacteriorhodopsin thin film," Phys. Rev. Lett. **95**, 253601 (2005).
9. H. Su, P. Kondratko, and S. L. Chuang, "Variable optical delay using population oscillation and four-wave-mixing in semiconductor optical amplifiers," Opt. Express **14**, 4800–4807 (2006).
10. J. Mørk, R. Kjær, M. van der Poel, and K. Yvind, "Slow light in a semiconductor waveguide at gigahertz frequencies," Opt. Express **13**, 8136–8145 (2005).
11. S. Melle, O. G. Calderón, F. Carreño, E. Cabrera, M. A. Antón, and S. Jarabo, "Effect of ion concentration on slow light propagation in highly doped erbium fibers," Opt. Commun. **279**, 53–63 (2007).
12. S. Melle, O. G. Calderón, C. E. Caro, E. Cabrera-Granado, M. A. Antón, and F. Carreño, "Modulation-frequency-controlled change from sub- to superluminal regime in highly doped erbium fibers," Opt. Lett. **33**, 827–829 (2008).
13. O. G. Calderón, S. Melle, M. A. Antón, F. Carreño, F. Arrieta-Yáñez, and E. Cabrera-Granado, "Propagation-induced transition from slow to fast light in highly doped erbium fibers," Phys. Rev. A **78**, 053812 (2008).
14. H. Shin, A. Schweinsberg, G. Gehring, K. Schwertz, H. J. Chang, R. W. Boyd, Q-H. Park, and D. J. Gauthier, "Reducing pulse distortion in fast light pulse propagation through an erbium doped fiber amplifier," Opt. Lett. **32**, 906–908 (2007).
15. H. Shin, A. Schweinsberg, and R. W. Boyd, "Reducing pulse distortion in fast-light pulse propagation through and erbium-doped fiber amplifier using a mutually incoherent background field," Opt. Commun. **282**, 2085–2087 (2009).
16. G. Piredda and R. W. Boyd, "Slow light by means of coherent population oscillations: laser linewidth effects," J. Eur. Opt. Soc. Rap. Commun. **2**, 07004 (2007).
17. F. Sanchez, P. L. Boudec, P.-L. Francois, and G. Stephan, "Effects of ion pairs on the dynamics of erbium-doped fiber lasers," Phys. Rev. A **48**, 2220–2229 (1993).
18. J. Li, K. Duan, Y. Wang, W. Zhao, J. Zhu, Y. Guo, and X. Lin, "Modeling and effects of ions pairs in high-concentration-erbium-doped fiber lasers," J. Mod. Opt. **55**, 447–458 (2008).
19. O. G. Calderón, S. Melle, F. Arrieta-Yáñez, M. A. Antón, and F. Carreño, "Effect of ion pairs in fast-light bandwidth in high-concentration erbium-doped fibers," J. Opt. Soc. Am. B **25**, C55–C60 (2008).
20. S. Wen and S. Chi, "Propagation characteristics of fast light in an erbium-doped fiber amplifier," J. Opt. Soc. Am. B **25**, 1073–1080 (2008).
21. S. Chin, M. Gonzalez-Herraez, and L. Thévanaz, "Zero-gain slow & fast light propagation in an optical fiber," Opt. Express **14**, 10684–10692 (2006).
22. S. S. Maicas, F. Öhman, J. Capmany, and J. Mørk, "Controlling microwave signals by means of slow and fast light effects in SOA-EA structures," IEEE Photon. Technol. Lett. **19**, 1589–1591 (2007).
23. F. G. Sedgwick, B. Pesala, J. Lin, W. S. Ko, X. Zhao, and C. J. Chang-Hasnain, "THz-bandwidth tunable slow light in semiconductor optical amplifiers," Opt. Express **15**, 747–753 (2007).
24. M. S. Bigelow, N. N. Lepeshkin, H. Shin, and R. W. Boyd, "Propagation of smooth and discontinuous pulses through materials with very large or very small group velocities," J. Phys. Condens. Matter **18**, 3117–3126 (2006).
25. B. Macke and B. Ségard, "Slow light in saturable absorbers," Phys. Rev. A **78**, 013817 (2008).